Ceramics International 42 (2016) 18338–18346

Contents lists available at ScienceDirect

Ceramics International

journal homepage: www.elsevier.com/locate/ceramint

Natural origin hydroxyapatite scaffold as potential bone tissue engineering substitute

Sudip Mondal [a,*], Umapada Pal [a], Apurba Dey [b]

[a] Instituto de Física, Benemérita Universidad Autónoma de Puebla, Apdo. Postal J-45, Puebla, Puebla 72570, Mexico
[b] Department of Biotechnology, National Institute of Technology Durgapur, M.G. Avenue, Durgapur 713209, Burdwan, West Bengal, India

ARTICLE INFO

Article history:
Received 18 July 2016
Received in revised form
21 August 2016
Accepted 25 August 2016
Available online 26 August 2016

Keywords:
Fish scale
Hydroxyapatite
Scaffold
Bone tissue

ABSTRACT

Fish scales derived natural hydroxyapatite (FS-HAp) scaffolds were prepared through solvent casting technique, which could mimic the structure of cortical and cancellous bone tissues of body system. The hydroxyapatite (HAp) biomaterial was synthesized by thermal decomposition of chemically treated fish scales. Fabricated scaffolds were characterized through morphological analysis, volumetric shrinkage, mechanical tests, and *in vitro*, *in vivo* biological studies. The projected scaffolds successfully mimic the cancellous/cortical bone system in terms of structure, porosity, mechanical strength, and exhibit excellent bioactive behavior. The FS-HAp scaffolds manifest good mechanical behaviors with Vickers Hardness (HV) of ~0.78 GPa, 0.52 GPa compressive stress, 190 MPa tensile stress and ~35% porosity on sintering at 1200 °C. *In vitro* and *in vivo* studies suggest these nontoxic HAp scaffolds graft with osteoconductive support, facilitating new cell growth on the developed scaffold surface. The graded grafts have a great potential for application as traumatized tissue augmentation substitute, and ideal for load-bearing bone applications.

1. Introduction

Musculoskeletal systems are becoming a major health concern for ageing population, congenital musculoskeletal disorder patients and accidental injuries. In human body system, bone is the second mostly implanted tissue after blood [1,2]. The use of bone grafts to treat, replace, or augment skeletal injuries and fractured bones was established by a great number of bone grafting scaffolds available at present. However, the exact combination of mechanically stable, bioactive, low cost scaffold materials required for these applications is still under investigation. Available biomaterials are of high cost due to their expensive synthetic routes or precursor chemicals. Moreover, their bioactivity is a major concern due to rejections in body system. Although the research in scaffold materials for hard tissue replacement had a huge success at laboratory scale during the last two decades, it is still thriving to get success in medical applications.

The major components of human bones are collagen and a substituted HAp (a natural bio-ceramic found in teeth). In human skeletal system, HAp is the most important thermodynamically stable calcium phosphate inorganic component in physiological condition. Potential applications of HAp include drug delivery, chromatography, catalyst, adsorptive matrix, bone tissue engineering [3]. The key advantages of synthetic HAp are its biocompatibility, deliberate biodegradability in physiological conditions with good osteoconductive and osteoinductive capabilities [4]. Taniguchi et al. demonstrated that sintered HAp exhibits excellent biocompatibility with soft tissues including skin, muscle and gums [5]. Synthetic HAp has also been widely used to repair hard tissues such as bone, bone augmentation, coating of implants or fillers for bone and teeth augmentation. The low mechanical strength of pure HAp ceramics is the only disadvantage for their application as load-bearing scaffold. Recent advances in science and technology of biomaterial synthesis and scaffold development have reignited the interest for HAp associated bone tissue engineering applications. This interdisciplinary engineering has concerned much attention as a new therapeutic means that may overcome the problems involved in the contemporary artificial prosthesis transplantation. Different synthetic routes such as wet chemical precipitation, sol-gel, hydrothermal synthesis, thermal decomposition, pyrolysis, sonochemical, mechanochemical, and biogenic sources have been applied [6,7] for HAp synthesis. Vats and coworkers performed clinical studies of different scaffold materials for tissue engineering applications [8]. Hollister et al. worked on the optimization of design and fabrication of scaffolds to mimic tissue properties for their successful biological applications [9]. Johnson et al. [10] studied and reviewed the compression, flexural and tensile properties of calcium phosphate (CaP) and CaP–polymer composites for applications in bone substitution

* Corresponding author.

http://dx.doi.org/10.1016/j.ceramint.2016.08.165
0272-8842/

and repair. Appleford et al. performed *in situ* studies of HAp scaffolds for bone tissue repair [11]. On the other hand, Tran et al. [12] demonstrated improved *in vitro* and *in vivo* osteoblast functions such as adhesion, proliferation, and synthesis of bone-related proteins and deposition of calcium containing minerals on nanostructured metals, ceramics, polymers, and composites.

In the present work, we adopted a new approach for developing strong, macroporous scaffolds from synthesized FS-HAp. Fish scales consist mainly of collagen proteins, connective tissue proteins and HAp crystals [13]. The process of extraction of HAp crystals are well documented in our previous article [14]. HAp powders were also synthesized by wet chemical precipitation, using calcium nitrate and diammonium hydrogen phosphate as precursor chemicals. The synthesized HAp powders were characterized by X-ray diffraction (XRD), Fourier transformed infrared (FTIR) spectroscopy, scanning electron microscopy (SEM) and energy dispersive spectroscopy (EDS) techniques. Synthesized HAp powders were utilized to develop porous scaffolds through solvent casting. Porosity and mechanical properties of the fabricated HAp scaffolds were associated to their good biological activities. With ~35% maximum porosity, the sintered FS-HAp scaffolds posse compressive strength of ~0.52 GPa, hardness of ~0.78 GPa and ~190 MPa tensile strength, which are within the range of cancellous bones. A new graft composition is developed, that could be a promising macroporous scaffold material to support *in situ* traumatized bone tissue. Compared to conventional bone tissue engineering scaffold materials, the new apatite scaffolds facilitate implant fixation and tissue ingrowth in hard tissue replacement applications. The results obtained on mechanical properties, cell culturing and *in situ* bone growth over these scaffold materials indicate their possible use as future bone prosthetic implants.

2. Experimental procedure

2.1. Synthesis of hydroxyapatite from fish scale

Tilapia fish (*Oreochromis mossambicus*) scales were collected and washed with tap water to remove attached undesired particles. To remove external hyaluronic acid and proteins, the initially washed scales were treated with 1 (N) NaOH (Sigma Aldrich) solution (2:1, v/w, NaOH Soln./fish scale) for 24 h at room temperature (25 ± 3 °C). The filtered fish scales are washed thoroughly with distilled water and dried at 50 °C in hot air oven for 6 h. Treated fish scales were calcined at 1200 °C for 2 h in air to obtain HAp bio-ceramics [15].

2.2. Synthesis of hydroxyapatite through chemical precipitation

Synthetic hydroxyapatite (SYN-HAp) powder was prepared by solution-precipitation method using calcium nitrate tetrahydrate [$Ca(NO_3)_2 \cdot 4H_2O$ (Sigma Aldrich)] and di ammonium hydrogen phosphate [$(NH_4)_2HPO_4$ (Sigma Aldrich)] as starting materials and ammonia solution [(NH_4OH, 28%) (Sigma Aldrich)] as precipitating agent [16].

A suspension of 0.24 M $Ca(NO_3)_2 \cdot 4H_2O$ [23.61 g $Ca(NO_3)_2 \cdot 4H_2O$ in 350 mL deionized water (18.2 Ω at 25 °C temperature)] was vigorously stirred at 40 °C. The pH of the solution was adjusted to 11.0 by adding drop-wise ammonia solution. Next another solution of 0.29 M $(NH_4)_2HPO_4$ [(7.92 g $(NH_4)_2HPO_4$ in 250 mL deionized water (18.2 Ω at 25 °C temperature)] was prepared. At 40 °C temperature freshly prepared 0.29 mL diammonium hydrogen phosphate solution was added drop-wise to the Ca $(NO_3)_2 \cdot 4H_2O$ solution. The transparent calcium nitrate solution became milky white in colour as the formation of HAp nanoparticles in the solution. The following reaction could be expressed as:

$$10Ca(NO_3)_2 \cdot 4H_2O + 6(NH_4)_2HPO_4 + 8NH_4OH \rightarrow Ca_{10}(PO_4)_6(OH)_2 + 20NH_4NO_3 + 20H_2O$$

The white precipitate was removed from the reaction solution by centrifugation at 5000 rpm for 6 min and dried at 80 °C. Obtained SYN-HAp powder was calcined in air at 1200 °C for 2 h.

2.3. Scaffold development

Solvent casting technique was employed to prepare porous HAp scaffolds (Fig. 1). First of all, 50 mL of 2% aqueous starch solution was prepared and synthesized HAp powders (either FS-HAp for FS-HAp scaffold or SYN-HAp for SYN-HAp scaffold) were added in steps to attain the desirable solids with 55 vol% loading. Insoluble starch (1 g) was added as porogen in this mixture. Next monomer, methacrylamide (MAM) 2.5 mL and cross-linker methylene bisacrylamide (MBAM) 0.5 mL was added. To initiate the chemical reactions 1 μL/g of slurries of ammonium persulphate (10% APS) was used. The total mixture of solutions and powders were milled in rotary milling machines for six (6) hours at 300 rpm speed. Finally, 0.5 μL/g of slurries and tetramethyl ethylenediamine (TEMED) were added to the mixture, which served as catalyst [17]. During mixing, some bubbles were formed in the slurry, and to avoid such uncontrolled bubble formation, octanol was used as de-foaming agent. The prepared slurry was finally casted into the desired mould and dried at controlled humidity at 50 °C for 48 h. After complete drying, the green bodies were removed from the mould and after measuring their sizes (diameter, width and height); they were sintered at 1200 °C temperature for 2 h in air atmosphere. After sintering, these scaffolds were tested to determine their shrinkage percentage. The same technique was employed for chemically synthesized HAp powder to prepare porous scaffolds.

3. Characterization

3.1. Characterization of HAp Powders

The calcined HAp powders were characterized by X-ray diffraction (XRD) using Cu Kα radiation (λ = 1.5405 Å) of a Bruker D8 Discover diffractometer, operating at 30 keV and 25 mA. FTIR analysis (PerkinElmer Spotlight 400 FT-IR) of the samples was performed in the 4000–400 cm^{-1} range to determine the functional groups present on their surface. Field-emission scanning electron microscopy (FE-SEM, SUPRA 40, CARLZEISSSMT, Oxford) and energy dispersive spectroscopy (EDS) analysis were performed to determine the morphology and composition of the samples, as well as to observe the pores developed in the scaffolds.

3.2. Mechanical characterizations of scaffold

3.2.1. Hardness

The Vickers test, a square-based pyramidal diamond indent was used, whose opposite sides met at the apex at an angle of 136° [18]. The diamond indent was pressed over the surface of the material at loads ranging up to approximately 0.5 Kgf. The size of the impression (maximum 0.5 mm) was measured with the aid of Wilson Vickers hardness testing machine.

The Vickers Hardness (HV) was calculated using the formula:

$$HV = \frac{F}{A} = \frac{1.8544F}{d^2}$$

where A is the surface area of resulting indentation in μm^2, d = the average length of the diagonal left by the indenter in μm, F = applied force in Kgf. Fully polished HAp samples with smooth

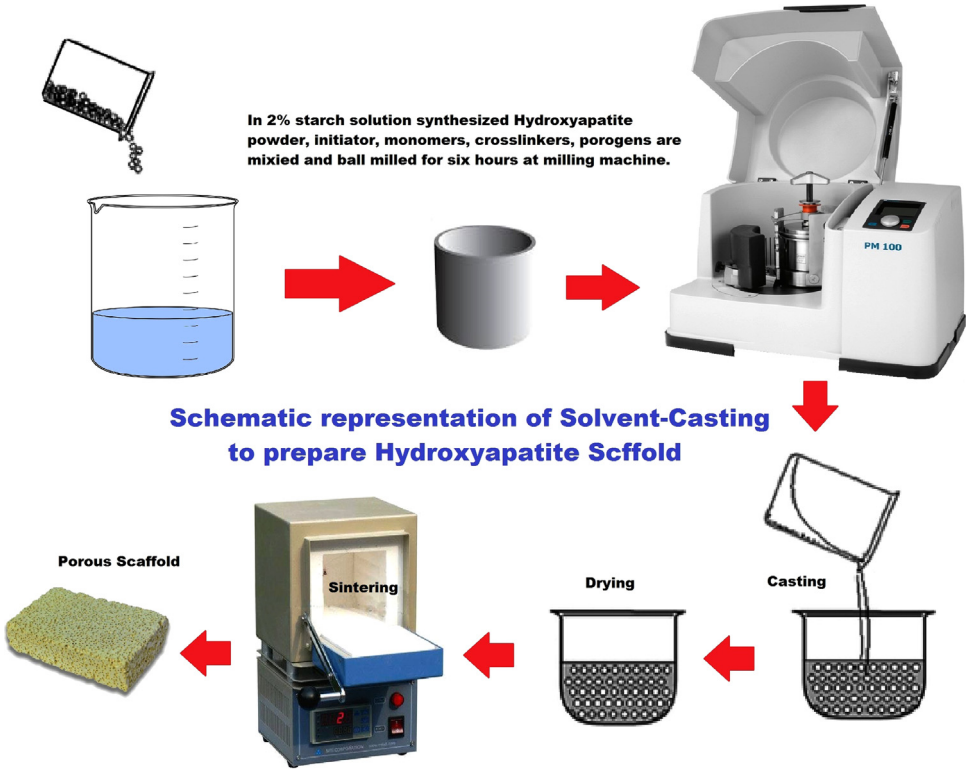

Fig. 1. Schematic representation of porous HAp scaffold development process by Solvent casting process.

reflecting surfaces were used for hardness study. The load used in the experiment was 0.5 kgf.

3.2.2. Compressive stress

The Compressive stress determination is an important criterion for bone fracture study [19]. The most common reasons for fractures are caused due to the compression type trauma. The utmost withstand capability of developed HAp scaffold may primarily important to determine the scaffold strength and it will helps to improve scaffold quality. All the samples for compressive tests are carried out by Instron Universal Testing Machine at a temperature of 25 ± 3 °C, and with relative humidity of 50 ± 5RH. The samples L/D ratio are between 4 and 6. Loads are applied on the compressive stress testing specimen with a speed rate of 0.2 mm/s.

3.2.3. Tensile stress

Properties of scaffold materials are usually expressed in terms of the stress–strain relationship of the material. The strength of a material is the breaking or ultimate strength under different modes of loading, such as tension, compression, torsion, or bending. The amount of energy liberated or absorbed during a tensile test is defined as the integral of the force and the displacement [19,20]. All the samples tensile tests are carried out by Instron Universal Testing Machine at a temperature of 25 ± 3 °C, and with relative humidity of 50 ± 5 RH. Force is applied on the tensile testing specimen with a speed rate of 0.2 mm/s.

3.2.4. Porosity

Porosity is a morphological property, which can be defined as the percentage of void space in solid samples [27]. The surface areas of porous bodies are much higher, which provide a good mechanical fixation on the surface, which allows chemical bonding and activity between the HAp scaffold and bones. A porous material may have both closed (isolated) pores and open (interconnected) pores. The interconnected pores look like tunnels and are accessible by biological fluids, gases and nutrients [28]. Pore interconnection provides the ways for cell distribution and migration which allows an efficient *in vivo* blood vessel formation. In this experimental study, porosity of HAp was measured by applying Archimedes' Principle.

$$\textit{Dry weight of the samples} = W_d,$$

$$\textit{Soaked weight of the samples} = W_s$$

$$\textit{Suspended weight of the samples} = W_d$$

$$\%\ \textit{Apparent Porosity} = \frac{W_s - W_d}{W_s - W_a} \times 100$$

3.3. Biological study of HAp powders and scaffolds

3.3.1. In vitro study (MTT Assay) of HAp powders

This colorimetric assay measures the reduction of yellow 3-(4, 5-dimethythiazol-2-yl)-2, 5-diphenyl tetrazolium bromide (MTT) by mitochondrial succinate dehydrogenase. The MTT enters the cells and passes into the mitochondria where it is reduced to an insoluble, coloured (dark purple) formazan product [21]. The conversion of MTT to formazan for FS-HAp and SYN-HAp is depicted in Fig. 5. The cells are then solubilised with an organic solvent (*e.g.* isopropanol) and the released, solubilised formazan reagent is measured spectrophotometrically. Since the reduction of MTT can only occur in metabolically active cells, the measurement of formazan represents the viability of the cells.

To perform the MTT [(3-(4,5-dimethylthiazol-2-yl)-2,5-diphenyltetrazolium-bromide)] assay, MG63 cell lines were seeded in 96 multi-well plates, at a 10^4 cell/cm^2 density in 100 μL of growth medium. After 24 h, the cells were exposed to the Fish scale derived HAp (FS-HAp) and chemically synthesized HAp (SYN-HAp) at a final concentration of 200 μg/mL for a period of 24, 48 and 72 h at 37 °C and 5% CO_2 atmosphere. Commercially purchased HAp was used as control in MTT assay study. After each incubation

time, the cells were incubated with 10 μL of a 0.5 mg/mL MTT solution for 4 h in the incubator. By the end of this period, the medium was removed and the produced formazan crystals were dissolved in 100 μL dimethyl sulfoxide (DMSO) [22].

The concentration of the coloured formazan was measured at 570 nm in a scanning multi-detection spectrophotometer micro plate reader (Biorad, USA). All the experiments were performed in triplicate. Cytotoxicity was expressed as a percentage of cell viability considering 100% viability in the control (cells treated with 1% DMSO in culture medium) using the relation:

$$\text{The percentage of cell viable} = \frac{\text{Absorbance of treated cells}}{\text{Absorbance of controlled cells}} \times 100\%$$

3.3.2. In vivo study of scaffold (implantation in rabbit model)

In the present study, all the animals (albino rabbit) were handled humanely, without making pain or distress, with due care for their welfare. Animals care and management were in complying with the regulations of the Committee for the Purpose of Control and Supervision of Experimental Animals (CPCSEA), Govt. of India. Institutional Animal Ethics Committee's approval was taken before initiating experiments with animals.

The implantation procedure was carried out under clean and aseptic conditions. Rabbits were anaesthetized using atropine (0.15 mg/kg), ketamine (90 mg/kg)+xylaxin (5 mg/kg body weight). The skins of anaesthetized rabbits were lightly swabbed using 70% alcohol, followed by betadine solution. The cortex region of femur was exposed and three holes of 2.0 mm size were drilled using low speed drill with profuse irrigation with saline. Three test materials (FS-HAp, SYN-HAp and control HAp) were implanted on the left leg femur bone and the wounds were closed by stitches. After the surgical procedure, all the animals were given post-operative care. The study was conducted in 8 rabbits, 4 animals for 1 week and 4 animals for 4 weeks. The body weight of all the animals was above 2 kg. At the end of the implantation period, the animals were euthanized by an overdose of anaesthetic agent. The test and the control implant materials along with the femur bone were collected. The sites of implantations were macroscopically examined for any evidence of tissue reaction. The collected test and control implanted materials along with femur bone were then fixed in 10% buffered formalin and were subjected to histopathological evaluation.

4. Results and discussions

4.1. HAp powders

4.1.1. XRD

XRD spectra of the HAp powders (FS-HAp and SYN-HAp) were compared with the standard JCPDS (# 00-024-0033) data of pure HAp (Fig. 2a). Sharp peaks appeared in the XRD patterns of the calcined HAp powders revealed their good crystallinity. Well-resolved characteristic peak of highest intensity was obtained at 2θ value of 31.77°, corresponding to (211) planes of HAp [13]. The average grain size of the HAp particles was estimated using Debye Scherer's relation over the most intense (002) peak:

$$D = 0.9\,\lambda/\beta\cos\theta$$

where, D represents average grain size, β stands for full width at half maximum of the peak, λ is the diffraction wavelength (0.154059 nm) and θ is the diffraction angle. The average crystallite size of the calcined HAp samples synthesized from fish scales and chemical route were 78.3 and 68.38 nm, respectively.

4.1.2. FTIR

The formation of apatite phase in FS-HAp and SYN-HAp powders was further confirmed by FTIR analysis (Fig. 2b). The FTIR spectra revealed a broad band centered in-between 1000 and 1100 cm^{-1} associated to the P–O bond of phosphate group. The major peaks at ~1028 and ~1088 cm^{-1} could be identified as symmetric n3 vibration of PO_4 group, which are the most intense peaks among the phosphate vibration modes. The other bands appeared around 965 and 560–650 cm^{-1} are the n1 and n4 symmetric P–O stretching vibrations of PO_4 group, respectively [23]. The distinguishable splitting of n4 vibration mode of PO_4 group was revealed in the FTIR band at ~596 and ~600 cm^{-1}. Appearance of these peaks in the FTIR spectra indicates the low site symmetry of molecules at two sites of the phosphate group in the HAp lattice. The bands assigned to the stretching mode of hydroxyl groups (O–H) in the HAp were observed at around 3567 cm^{-1} for both FS-HAp and SYN-HAp samples [24,25]. Appearance of sharp peaks associated to stretching vibration in the investigated samples indicates the formation of crystalline HAp.

4.1.3. SEM and EDS

Formation of well-dispersed, nearly spherical HAp nanoparticles can be observed in the SEM image presented in Fig. 3. The average particle size of FS-HAp and SYN-HAp powders determined

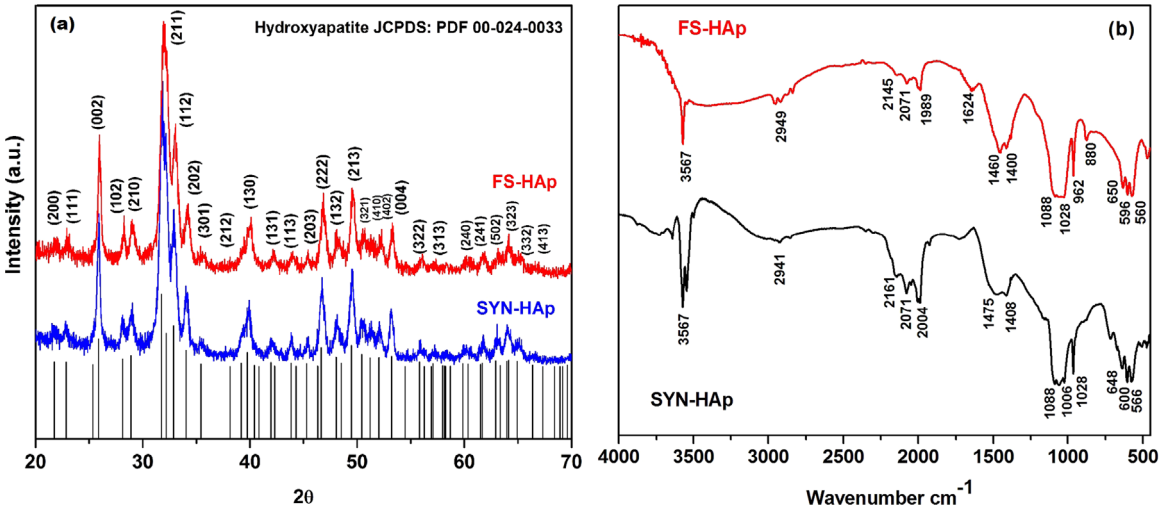

Fig. 2. (a) XRD and (b) FTIR analysis of synthesized FS-HAp powder.

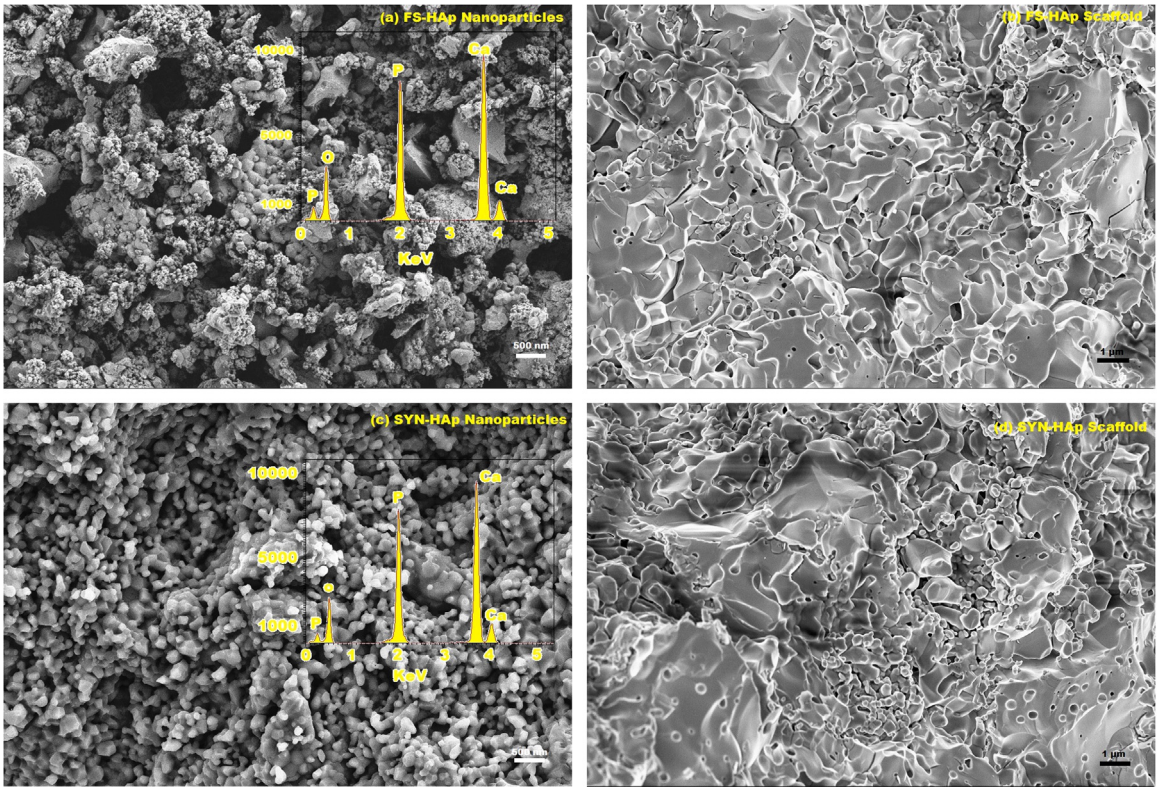

Fig. 3. SEM and EDS analysis of FS-HAp and SYN-HAp nanoparticles and their corresponding scaffolds.

from these micrographs were ~182 nm and ~106 nm, respectively. Ca/P atomic ratios in the synthesized FS-HAp and SYN-HAp powders determined through EDS analysis were 1.61 and 1.65, respectively.

In this study, we used three different types of scaffold for hardness, compressive stress and tensile stress analysis. Use of three different types of mould produced scaffolds of three different shapes. ASTM F2883-11 standards were followed for the characterization of ceramic and mineral-based scaffolds used for tissue-engineered medical products (TEMPs) and as devices for surgical implant applications [26]. For Hardness testing, small HAp pellet scaffolds of 12 mm diameter and 6 mm height were prepared. The compressive strength scaffold was of cylindrical shape, with a diameter of 3 cm and 2.5 cm height. For tensile stress measurement, a dumbbell shaped specimen of 12 mm thick, 20 mm wide and 16.5 cm long gauge section was prepared (Fig. 4).

4.2. Mechanical characterizations and properties of developed scaffolds

The FS-HAp and SYN-HAp powders were utilized for porous HAp scaffold development by solvent casting method. The developed scaffolds were sintered in air at different temperatures in between 800 and 1400 °C for one h, and studied further to determine their mechanical stability and biological responses.

4.2.1. Hardness

The hardness value significantly increases with increase in sintering temperature (Fig. 5). The rate of increase in hardness depends on the nature of material. Initially, on sintering at 800 °C, FS-HAp and SYN-HAp shows ~0.78 GPa and ~0.76 GPa hardness, respectively. On increasing the sintering temperature to 1200 °C, there is subsequent increase in hardness for all the HAp scaffolds. The hardness of 1200 °C sintered FS-HAp and SYN-HAp scaffolds were estimated to be 1.09 GPa and 1.03 GPa, respectively. On increasing the sintering temperature up to 1300 °C, the hardness of FS-HAp and SYN-HAp scaffold increased to ~1.29 GPa and ~1.28 GPa, respectively. The hardness value of FS-HAp and SYN-HAp scaffolds increased and remained almost same (~1.30 GPa) on sintering at 1400 °C. As can be seen from Fig. 5, on sintering beyond 1200 °C, the hardness of FS-HAp and SYN-HAp scaffolds do not increase proportionately. Moreover, the hardness of both the samples turnout to be same. This may be due to slow decomposition of carbonated FS-HAp at higher sintering temperatures, leading its morphology same as the morphology of SYN-HAp scaffolds.

4.2.2. Tensile stress

The tensile strength of all the scaffolds increased with the increase of sintering temperature. The FS-HAp scaffold showed better tensile strength of approximately ~190 MPa at 1200 °C temperature compared to SYN-HAp scaffold (~182 MPa). The FS-HAp scaffold shows highest tensile strength of about ~195 MPa at 1400 °C (Fig. 5). However, the tensile strength of the fabricated scaffolds did not increase further on increasing the sintering temperature beyond 1250 °C. Therefore, a sintering temperature in between 1200 and 1250 °C seems optimum for fabricating HAp scaffolds.

4.2.3. Compressive stress

The rate of increasing compressive stress depends upon the properties of materials and processing temperature (Fig. 5). The maximum compressive stress was recorded for FS-HAp scaffold sintered at 1200 °C. After sintering at 1200 °C, the compressive stresses of FS-HAp and SYN-HAp were estimated to be ~520 MPa and ~507 MPa, respectively. The ultimate compressive strength of the developed FS-HAp scaffold had reached up to ~560 MPa at higher sintering temperature, which is almost similar to the compressive stress of SYN-HAp scaffold (~564 MPa). For sintering above 1200 °C, the compressive stress value of SYN-HAp scaffold

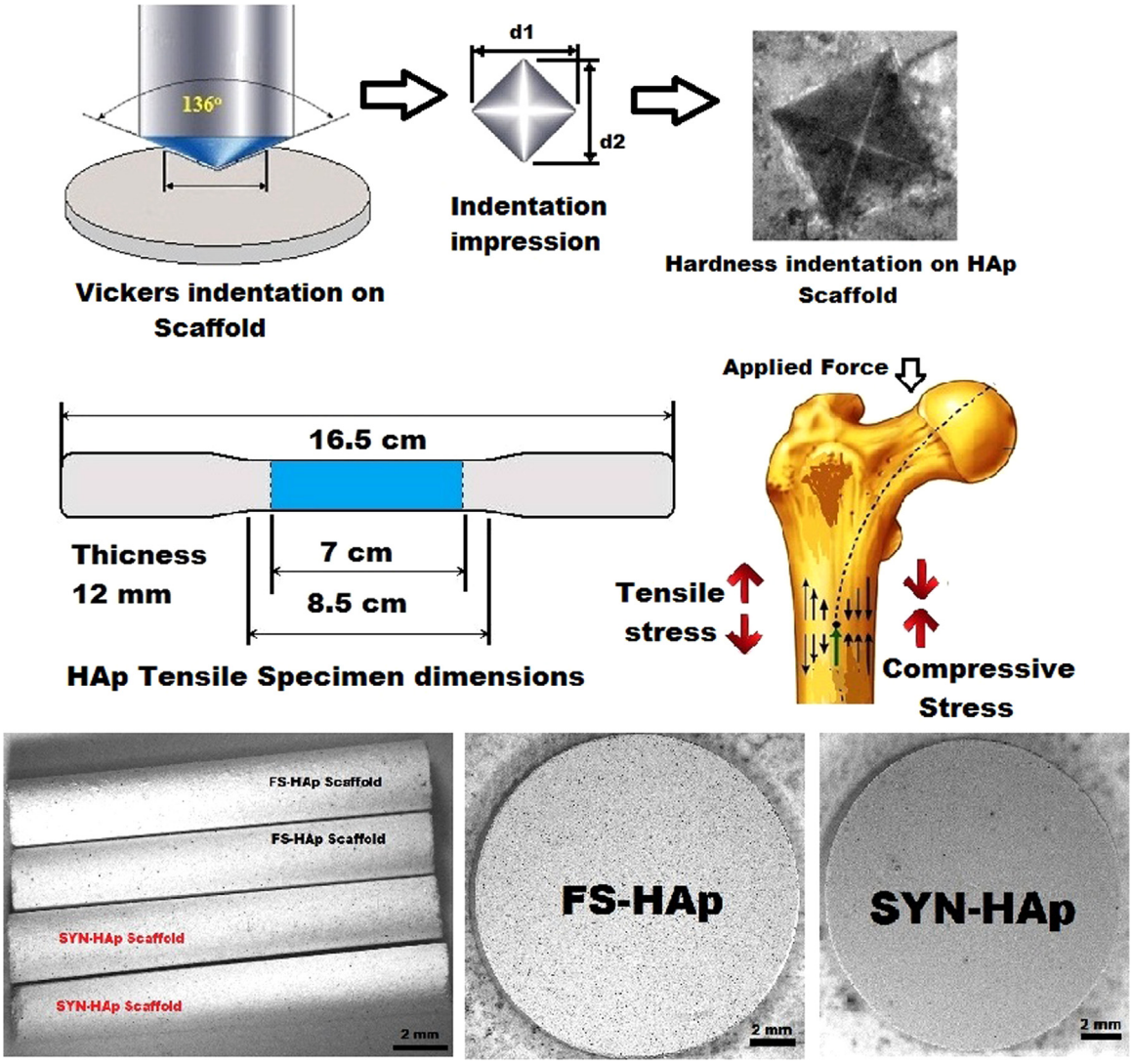

Fig. 4. Schematics of used mechanical characterization process over the developed HAp scaffolds.

was a little higher than that of FS-HAp scaffold. This might be due to the decomposition of FS-HAp at higher sintering temperature leading to a morphological change of FS-HAp particles. The experimental tensile and compressive behaviors of the developed scaffolds were compared with the mechanical data of different bone species and biomaterials reported in the literature, and presented in Table 1.

4.2.4. Porosity

The sintered HAp scaffold surfaces revealed porous structures with interconnected network. The microstructural study of the solvent casted sintered scaffolds showed noticeable porosity of ~30–35%, which could be useful for biomedical applications as fillers or scaffolds. The SEM analysis also shows porous structure on developed HAp scaffold surface. The morphology of the synthesized HAp nanoparticles is totally different with developed scaffold surface. In the scaffold materials all the particles are fused due to sintering at higher temperature and make porous structure due to the melting and evaporation of porogens.

4.2.5. Shrinkage

Shrinkage occurs when a sample contains lots of water or evaporative agents. Due to evaporation, the unoccupied space is filled by surrounding materials, causing shrinkage. Evaporation induced shrinkage along with grain boundary merging have been observed due to sintering. Evaporation induced shrinkage might also produce major defects in scaffolds along with shape deformation [29]. To prevent shrinkage in our developed scaffolds, we always maintain a good solid loading and optimum porogen ratio. In our study, the scaffolds made of FS-HAp particles exhibited very low shrinkage (3.15% at 1200 °C) in comparison with the scaffolds made of chemically synthesized HAp particles (5.41% at 1200 °C).

4.3. Biological evaluations

4.3.1. MTT Assay

MTT assay results (Fig. 6) suggest that some of HAp particles have inhibitory effect on the growth of the cells compared to the control. FS-HAp particle containing culture shows almost similar viability as that of control cell lines. The study was performed up to 72 h and spectrometric study was performed after every 24 h interval. In day 1, the control cell line shows maximum proliferation of cells. FS-HAp and SYN-HAp shows almost similar viability but much less than control. This might have occurred due to the presence of irregular shaped HAp particles, which obstacles the proliferation of new cells.

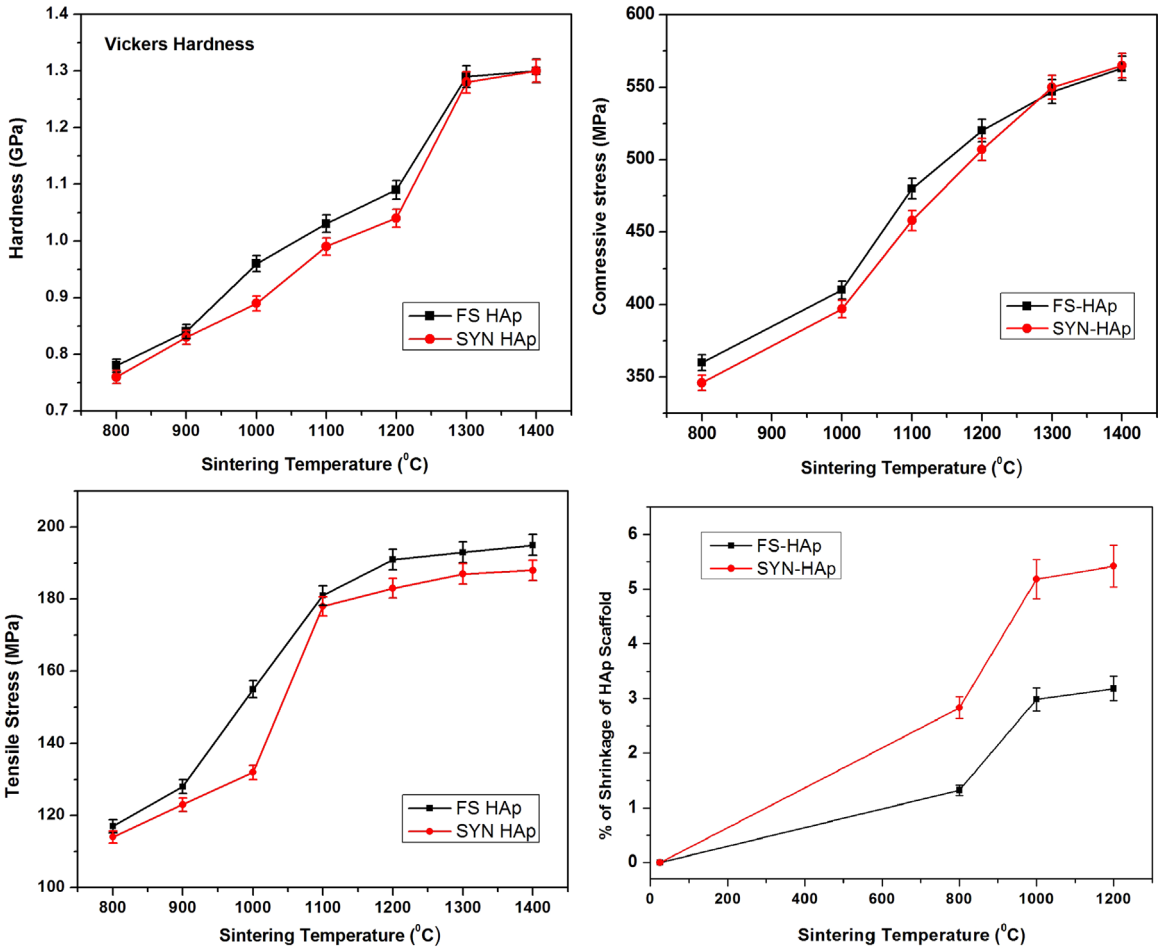

Fig. 5. Variation of (a) hardness, (b) tensile stress, (c) compressive stress and (d) shrinkage behavior of the developed HAp scaffolds.

Table 1
Mechanical properties of bones and biomaterials of different origin.

Materials	Tensile strength (MPa)	Compressive strength (MPa)	References
Human	50–151	130–200	[30,31,32]
Cattle	100–136	141–161	[20]
Pig	80–112	99–109	[20]
Horse	100–123	143–163	[20]
Bioglass® 45S5	42	500	[30,33]
FS-HAp scaffold (sintered 1200 °C)	190	520	Present Study
SYN-HAp scaffold (sintered 1200 °C)	182	507	Present Study

4.3.2. *Histological analysis*

The microscopic view of the sample (FS-HAp scaffold) clearly indicates the healing regions. Operated areas are being recovered by healing new cells as cell infiltration on materials was observed. Deeply stained region may conclude the presence of pre-osteoblast cells because this type of cells consists of mono nucleus with prominent nucleoli. In some regions, new cell linings appeared, which might be the result of osteoconduction. New bone cell formation in traumatized regions shows good bio-affinity and osteoconductive characteristics of FS-HAp biomaterial (Yellow arrow in Fig. 7(a)). In case of SYN-HAp scaffold implantation, cell infiltration occurs in the healing region but the rate of recovery is low. In respect with FS-HAp the osteo-integration property of SYN-HAp is very poor (Yellow arrow in Fig. 7(b)). The synthetic route of HAp preparation in chemical solution may increase the risk of contamination of different ions. Probably due to this reason, the osteo-integration property was hampered for this type (SYN-HAp) of particles when integrated inside the animal body system.

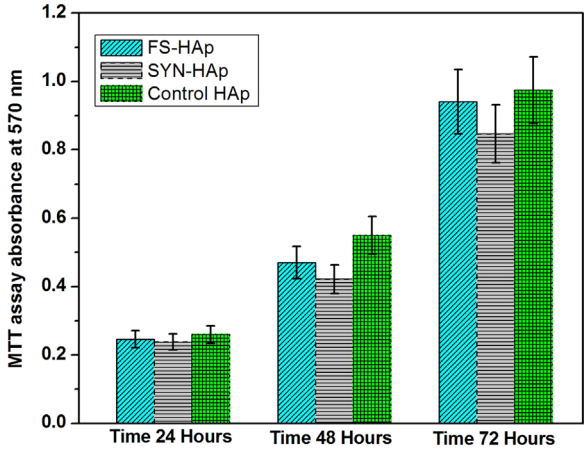

Fig. 6. Biological *in vitro* evaluation (MTT assay) of synthesized HAp powders compared with commercial HAp.

5. Conclusions

In summary, HAp biomaterials were successfully synthesized from natural source like fish scale and through chemical precipitation method. To apply these HAp biomaterials for bone tissue

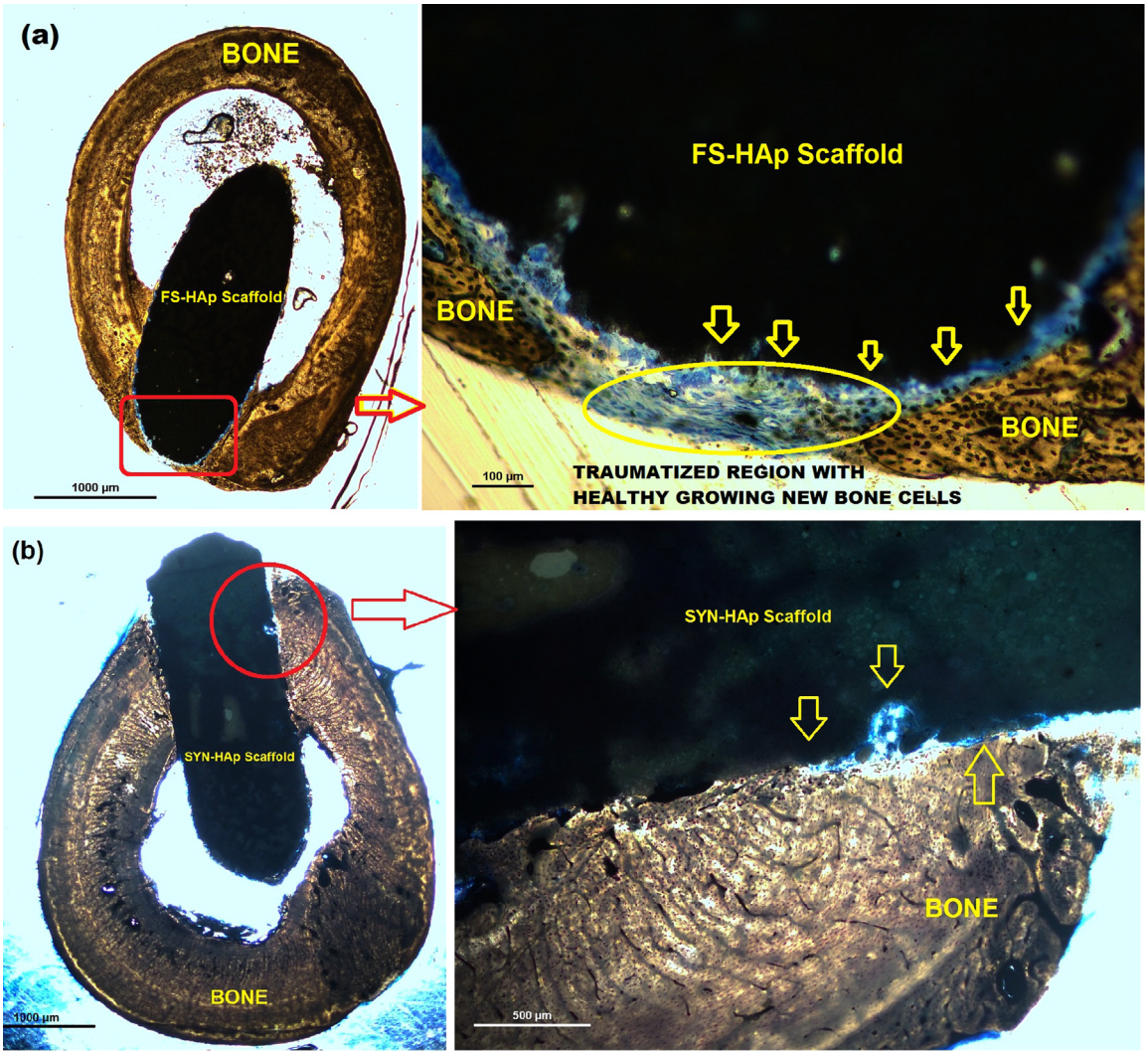

Fig. 7. Biological *in vivo* implantation study of the developed HAp scaffolds. (For interpretation of the references to color in this figure legend, the reader is referred to the web version of this article.)

engineering, their morphology, crystallinity, and composition were evaluated. It has been observed that both the FS-HAp and SYN-HAp biomaterials are well crystalline, with stoichiometry very similar to natural HAp. The scaffolds fabricated with FS-HAp and SYN-HAp exhibit porous structure, which facilitates blood, essential body fluids, nutrients and gases to flow through it. The porous structure also helps to adhere and proliferate new bone cells throughout the scaffold. With better mechanical properties in terms of hardness, compressive stress and tensile stress, the FS-HAp scaffolds provide better substitute for traumatized hard tissue replacement. The cytotoxicity assay of synthesized FS-HAp and SYN-HAp biomaterials shows no significant toxic effect. The MTT assay of FS-HAp nanoparticles shows better cell proliferation comparing to SYN-HAp nanoparticles. The same phenomenon is also observed when FS-HAp and SYN-HAp scaffolds are studied in animal models. The healing rate for implanted FS-HAp scaffold is better and faster than SYN-HAp scaffold. *In vivo* histological analysis revealed new bone cells formation occurs in between the trauma region of both developed HAp scaffolds and host bone. The proliferated new cells are viable and healthy. For FS-HAp scaffold, the cells are almost covers the surgical gaps in between scaffold and host bone. The developed porous FS-HAp scaffold with excellent bioactivity is expected to be a promising load-bearing bone substitute in clinical practice.

Acknowledgements

SM is thankful to CSIR, Government of India, for financial support [SRF fellowship (File No. 31/19 (6)/2012-EMR-I)]. SM is also thankful to the Secretaria de Educación Publica, Mexico, for offering PRODEP-SEP postdoctoral fellowship (Offer No. DSA/103.5/15/8164).

References

[1] M.E. Elsalanty, D.G. Genecov, Bone grafts in craniofacial surgery, craniomaxillofac, Trauma Reconstr. 2 (2009) 125–134.
[2] A. Oryan, S. Alidadi, A. Moshiri, N. Maffulli, Bone regenerative medicine: classic options, novel strategies, and future directions, J. Orthop. Surg. Res. 9 (2014) 1–27.
[3] H. Zhou, J. Lee, Nanoscale hydroxyapatite particles for bone tissue engineering, Acta Biomater. 7 (2011) 2769–2781.
[4] R.Z. Legeros, Biodegradation and bioresorption of calcium phosphate ceramics, Clin. Mater. 14 (1993) 65–88.
[5] M. Taniguchi, H. Takeyema, I. Mizunna, N. Shinagawa, J. Yura, N. Yoshikawa, H. Aoki, The clinical application of intravenous catheter with percutaneous device made of sintered hydroxyapatite, Jpn. J. Artif. Organs 20 (1991) 460–464.
[6] M.S. Shojai, M.T. Khorasani, E.D. Khoshdargi, A. Jamshidi, Synthesis methods for nanosized hydroxyapatite with diverse structures, Acta Biomater. 9 (2013) 7591–7621.
[7] S.V. Dorozhkin, Nanodimensional and nanocrystalline apatites and other

calcium orthophosphates in biomedical engineering, biology and medicine, Materials 2 (2009) 1975–2045.
[8] A. Vats, N.S. Tolley, J.M. Polak, J.E. Gough, Scaffolds and biomaterials for tissue engineering: a review of clinical applications, Clin. Otolaryngol. Allied Sci. 28 (2003) 165–172.
[9] S.J. Hollister, R.D. Maddox, J.M. Taboas, Optimal design and fabrication of scaffolds to mimic tissue properties and satisfy biological constraints, Biomaterials 23 (2002) 4095–4103.
[10] A.J.W. Johnson, B.A. Herschler, A review of the mechanical behavior of CaP and CaP/polymer composites for applications in bone replacement and repair, Acta Biomater. 7 (2011) 16–30.
[11] M.R. Appleford, S. Oh, N. Oh, J.L. Ong, In vivo study on hydroxyapatite scaffolds with trabecular architecture for bone repair, J. Biomed. Mater. Res. A 89 (2009) 1019–1027.
[12] N. Tran, T.J. Webster, Nanotechnology for bone materials, Nanomed. Nanobiotechnol. 1 (2009) 336–351.
[13] S. Mondal, S. Mahata, S. Kundu, B. Mondal, Processing of natural resourced hydroxyapatite ceramics from fish scale, Adv. Appl. Ceram. 109 (2010) 234–239.
[14] S. Mondal, R. Bardhan, B. Mondal, A. Dey, S.S. Mukhopadhyay, R. Guha, K. Roy, S. Roy, Synthesis, characterization and in vitro cytotoxicity assessment of hydroxyapatite from different bio sources for Tissue engineering application, Bull. Mater. Sci. 35 (2012) 683–691.
[15] S. Mondal, B. Mondal, A. Dey, S.S. Mukhopadhyay, Studies on processing and characterization of hydroxyapatite biomaterials from different bio wastes, J. Miner. Mater. Charact. Eng. 11 (2012) 55–67.
[16] F. BaKan, O. lacin, H. Sarac, A novel low temperature sol–gel synthesis process for thermally stable nano crystalline hydroxyapatite, Powder Technol. 233 (2013) 295–302.
[17] S. Dhara, R.K. Kamboj, M. Pradhan, P. Bhargava, Shape forming of ceramics via gelcasting of aqueous particulate slurries, Bull. Mater. Sci. 25 (2002) 565–568.
[18] ASTM E384-11e1, Standard Test Method for Knoop and Vickers Hardness of Materials, American society for testing and materials international. ⟨www.astm.org⟩.
[19] R.O. Ritchie, K.J. Koester, S. Ionova, W. Yao, N.E. Lane, J.W. Ager, Measurement of the toughness of bone: A tutorial with special reference to small animal studies, Bone 43 (2008) 798–812.
[20] S. Pal, Design of Artificial Human Joints & Organs, Springer, US, 2014, http://dx.doi.org/10.1007/978-1-4614–6255-2, eBook ISBN:978-1-4614–6255-2.
[21] J.C. Stockert, A.B. Castro, M. Cañete, R.W. Horobin, A. Villanueva, MTT assay for cell viability: Intracellular localization of the formazan product is in lipid droplets, Acta Histochem. 114 (2012) 785–796.
[22] M. Kinugawa, S. Fukuzawa, K. Tachibana, Skeletal protein protection: the mode of action of an anti-osteoporotic marine alkaloid, norzoanthamine, J. Bone Miner. Metab. 27 (2009) 303–314.
[23] M.H. Fathi, A. Hanifi, V. Mortazav, Preparation and bioactivity evaluation of bone-like hydroxyapatite nano powder, J. Mater. Process. Technol. 202 (2008) 536–542.
[24] S. Raynaud, E. Champion, D. Bernache-Assollant, P. Thomas, Calcium phosphate apatites with variable Ca/P atomic ratio I. Synthesis, characterisation and thermal stability of powders, Biomaterials 23 (2002) 1065–1072.
[25] T. Kokubo, Surface chemistry of bioactive glass-ceramics, J. Non-Cryst. Solids 120 (1990) 138–151.
[26] ASTM F2883-11, Standard guide for characterization of ceramic and mineral based scaffolds used for tissue-engineered medical products (TEMPs) and as device for surgical implant applications, ASTM International, West Conshohocken, PA, 2011. ⟨www.astm.org⟩.
[27] G. Krishnamurithy, M.G. Murali, M. Hamdi, A.A. Abbas, H.B. Raghavendran, T. Kamarul, Characterization of bovine-derived porous hydroxyapatite scaffold and its potential to support osteogenic differentiation of human bone marrow derived mesenchymal stem cells, Ceram. Int. 40 (2014) 771–777.
[28] S. Mondal, A. Mondal, B. Mondal, N. Mandal, A. Dey, S.S. Mukhopadhyay, S. Singh, Physico-chemical characterization and biological response of Labeorohita-derived hydroxyapatite scaffold, Bioprocess Biosyst. Eng. 37 (2014) 1233–1240.
[29] I. Sabree, J.E. Gough, B. Derby, Shrinkage may cause major defects and also makes faulty shapes, Ceram. Int. 41 (2015) 8425–8432.
[30] K. Rezwan, Q.Z. Chen, J.J. Blaker, A.R. Boccaccini, Biodegradable and bioactive porous polymer/inorganic composite scaffolds for bone tissue engineering, Biomaterials 27 (2006) 3413–3431.
[31] C.J. Hernandez, G.S. Beaupre, T.S. Keller, D.R. Carter, The influence of bone volume fraction and ash fraction on bone strength and modulus, Bone 29 (2001) 74–78.
[32] L.C. Gerhardt, A.R. Boccaccini, Bioactive glass and glass-ceramic scaffolds for bone tissue engineering, Materials 3 (2010) 3867–3910.
[33] T. Nakamura, T. Yamamuro, S. Higashi, T. Kokubo, S. Itoo, A new glass-ceramic for bone replacement-evaluation of its bonding to bone, J. Biomed. Mater. Res. 19 (1985) 685–698.